AD-A148 766 THE INFLUENCE OF POROSITY ON THE DEFORMATION AND FRACTURE OF ALLOYS(U) MICHIGAN TECHNOLOGICAL UNIV HOUGHTON DEPT OF METALLURGICAL EN.. 1/1

UNCLASSIFIED R J BOURCIER ET AL. NOV 84 TR-26 F/G 11/6 NL

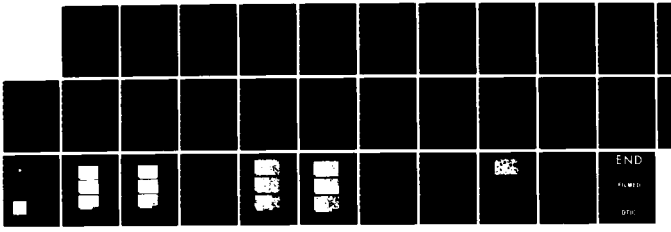

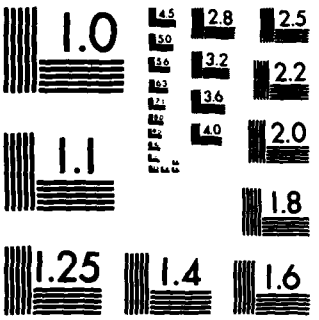

MICROCOPY RESOLUTION TEST CHART
NATIONAL BUREAU OF STANDARDS-1963-A

(12)

AD-A148 766

TECHNICAL REPORT NO. 26

TO

THE OFFICE OF NAVAL RESEARCH
CONTRACT No. N00014-76-C-0037, NR 031-756

THE INFLUENCE OF POROSITY ON THE DEFORMATION AND FRACTURE OF ALLOYS

R. J. BOURCIER[+$], D. A. KOSS[+],
R. E. SMELSER[*], AND O. RICHMOND[*]

[+]DEPARTMENT OF METALLURGICAL ENGINEERING
MICHIGAN TECHNOLOGICAL UNIVERSITY
HOUGHTON, MI 49931

[*]CURRENTLY WITH ALCOA TECHNICAL CENTER,
ALCOA CENTER, PA 15069

[$]CURRENTLY WITH SANDIA NATIONAL LABORATORIES,
ALBUQUERQUE, NM 87185

DTIC FILE COPY

DEC 7 1984
E

REPRODUCTION IN WHOLE OR IN PART IS PERMITTED FOR ANY PURPOSE OF THE UNITED STATES GOVERNMENT. DISTRIBUTION OF THIS DOCUMENT IS UNLIMITED.

84 12 13 054

SECURITY CLASSIFICATION OF THIS PAGE (When Data Entered)

REPORT DOCUMENTATION PAGE		READ INSTRUCTIONS BEFORE COMPLETING FORM
1. REPORT NUMBER No. 26	2. GOVT ACCESSION NO. AD-A148766	3. RECIPIENT'S CATALOG NUMBER
4. TITLE (and Subtitle) The Influence of Porosity on the Deformation and Fracture of Alloys		5. TYPE OF REPORT & PERIOD COVERED 6. PERFORMING ORG. REPORT NUMBER
7. AUTHOR(s) R. J. Bourcier, D. A. Koss, R. E. Smelser, and O. Richmond		8. CONTRACT OR GRANT NUMBER(s) N00014-76-C-0037 NR031-756
9. PERFORMING ORGANIZATION NAME AND ADDRESS Department of Metallurgical Engineering Michigan Technological University Houghton, MI 49931		10. PROGRAM ELEMENT, PROJECT, TASK AREA & WORK UNIT NUMBERS
11. CONTROLLING OFFICE NAME AND ADDRESS Office of Naval Research 800 N. Quincy St. Arlington, VA 22217		12. REPORT DATE November 1984 13. NUMBER OF PAGES 22
14. MONITORING AGENCY NAME & ADDRESS(if different from Controlling Office)		15. SECURITY CLASS. (of this report) Unclassified 15a. DECLASSIFICATION/DOWNGRADING SCHEDULE

16. DISTRIBUTION STATEMENT (of this Report)

Distribution of this document is unlimited

17. DISTRIBUTION STATEMENT (of the abstract entered in Block 20, if different from Report)

18. SUPPLEMENTARY NOTES

19. KEY WORDS (Continue on reverse side if necessary and identify by block number)

Deformation, fracture, porosity, titanium, Ti-6Al-4V

TITANIUM-6ALUMINUM-4VANADIUM

20. ABSTRACT (Continue on reverse side if necessary and identify by block number)

The tensile deformation and fracture behavior of alloys containing rounded porosity and with differing levels of matrix strain hardening has been examined both experimentally and analytically. The stress-strain response in uniaxial tension and, to a limited extent, plane-strain tension has been determined at room temperature for powder-fabricated ~~Ti~~ and ~~Ti-6Al-4V~~ containing porosity. The strength and the ductility of both alloys decrease substantially with increasing porosity level. A large strain elastoplastic finite element model

DD FORM 1 JAN 73 1473 EDITION OF 1 NOV 65 IS OBSOLETE
S/N 0102-LF-014-6601

SECURITY CLASSIFICATION OF THIS PAGE (When Data Entered)

based on a regular array of equal-sized spherical voids is used to predict bulk porosity effects; the analysis is in good agreement with the experimentally observed rates of void growth, but it underestimates the degradation of strength with increasing porosity. In an analysis unique to P/M alloys, the effects of porosity on a local scale are examined successfully by a continuum imperfection model which predicts the fracture of porous materials with differing matrix strain-hardening characteristics. The analysis is significant in that it implies that a primary effect of porosity on fracture is to introduce into the material a network of planes of high local pore content ("imperfections").

Accession For	
NTIS GRA&I	X
DTIC TAB	☐
Unannounced	☐
Justification	
By	
Distribution/	
Availability Codes	
Dist | Avail and/or Special	
A-1	

The Influence of Porosity on the Deformation and Fracture of Alloys

R. J. Bourcier[†$], D. A. Koss[†],
R. E. Smelser[°*], and O. Richmond[°*]

[†]Department of Metallurgical Engineering
Michigan Technological University
Houghton, Michigan 49931

[°]Research Laboratory
U.S. Steel Corporation
Monroeville, Pennsylvania 15146

[*]Currently with Alcoa Technical Center,
Alcoa Center, Pennsylvania 15069

[$]Currently with Sandia National Laboratories
Albuquerque, NM 87185

Abstract

The tensile deformation and fracture behavior of alloys containing rounded porosity and with differing levels of matrix strain hardening has been examined both experimentally and analytically. The stress-strain response in uniaxial tension and, to a limited extent, plane-strain tension has been determined at room temperature for powder-fabricated Ti and Ti-6Al-4V containing porosity. The strength and the ductility of both alloys decrease substantially with increasing porosity level. A large strain elastoplastic finite element model based on a regular array of equal-sized spherical voids is used to predict bulk porosity effects; the analysis is in good agreement with the experimentally observed rates of void growth, but it underestimates the degradation of strength with increasing porosity. In an analysis unique to P/M alloys, the effects of porosity on a local scale are examined successfully by a continuum imperfection model which predicts the fracture of porous materials with differing matrix strain-hardening characteristics. The analysis is significant in that it implies that a primary effect of porosity on fracture is to introduce into the material a network of planes of high local pore content ("imperfections").

INTRODUCTION

Ductile fracture in engineering alloys is usually the result of the nucleation, growth and link-up of voids or cavities. In fully dense materials, voids are formed during straining, usually by the decohesion or fracture of large inclusions or precipitates (for a review, see Goods and Brown (1)). While the statistical nature of void formation results in cavities being nucleated over a range of strains, void nucleation in most alloys begins early in the deformation process, and as a result the fracture behavior is controlled by void growth and void link-up. Furthermore, many technologically important materials contain pre-existing porosity, such as may be present in castings and powder metallurgy (P/M) consolidated alloys. The present research is an examination of the effects of pre-existing porosity and of matrix strain hardening on the deformation and fracture of high strength engineering alloys in general and of two P/M Ti alloys in particular.

The influence of porosity on plastic flow and instability/fracture has been studied experimentally (for a review, see refs. 2 and 3), with physical models (5-8), with simple models based on elastic stress concentrations and porosity level/geometry in sintered metals (9-15), and with mathematical models (for example, see refs. 16-21). A limitation of previous studies is that little critical comparison has been made between models which take into account plasticity and the observed flow and fracture behavior of the porous material. The result is that the validity of the modeling techniques (especially at large strains) remains unproven, and no basis exists to suggest modifications or improvements. The purpose of this study is not only to identify the parameters which control the deformation and fracture of porous or cavitating alloys but also to relate these to experimental data. In particular, we shall distinguish between behavior which may be adequately

interpreted in terms of bulk porosity content and that which is dominated by planes of high local pore content.

The experimental aspects of the study are based on the contrasting deformation and fracture behavior of two Ti alloys, commercially pure (CP) Ti and Ti-6Al-4V, which possess considerably different strain hardening characteristics and which have been consolidated via P/M techniques to similar levels of rounded and mostly isolated porosity. The yielding, flow, void growth and void link-up behavior are examined experimentally, and metallographic and fractographic analyses are used to define the bases for quantitative model formulations. The analyses distinguish between that behavior which can be interpreted on the basis of bulk porosity content as compared to that which must be interpreted on the basis of local pore content. For the former approach, a large strain elastoplastic finite element model (22) based on a "microcell" approach is used. A contrasting approach is that porosity (or strain-induced voids) introduces into the material planes of high local pore content: "imperfections". The continuum analysis of Saje, Pan, and Needleman (23) may be used to predict the fracture behavior of alloys containing such imperfections including the effects of matrix strain hardening.

THEORETICAL AND EXPERIMENTAL PROCEDURES

Finite Element Modeling of the Plastic Deformation of a Porous Material

The goal of the finite element (FE) modeling portion of this study was to examine the influence of various initial levels of bulk porosity on yielding and on subsequent stable flow behavior (not including fracture). In order to obtain a geometric symmetry for FE modeling, it was assumed that the dispersion of pores which exists in the P/M materials can be replaced by a periodic regular array of equal sized voids with an AAA... stacking sequence; Fig. 1 shows a schematic illustration of the assumptions made in applying FE modeling

to the P/M materials. To reduce the problem to one which might be treated in two dimensions, the periodic array is subdivided into a regular array of individual cells with the porosity equal to the bulk porosity content of the material as indicated in Fig. 1b. One of these cells is then transformed into a right circular cylinder (whose height is equal to its diameter) containing a central cavity, Fig. 1c. This "microcell" (22) was felt to be a reasonable approximation of a three dimensional structure while still using a two dimensional calculation scheme. An example of the resulting mesh, consisting of 880 triangular elements, as well as the boundary conditions used is shown in Fig. 1d. In order to examine the possible influence of pore shape on void growth, both prolate and oblate spheroids, with aspect ratios of 2.0 and 0.5, respectively, were substituted for the spherical cavity in modeling of the 4.5% porous CP Ti material for comparison with experimental density change measurements.The FE analyses were performed using the large strain elasto-plastic program FIPAX (23) for isotropic work hardening materials.

Continuum Imperfection Modeling of Failure of a Porous Material

Previous research (22) has indicated that the regular array models are too stiff to analyze the plastic flow localization and failure process caused by variations of local pore content: specifically, planes of high pore content or "imperfections". It was thus decided to use continuum flow localization models for this purpose. In order to examine the influence of non-uniformity of pore distribution, the continuum imperfection analysis of Yamamoto (25), as modified by Saje, Pan and Needleman (23) for tensile necking, was used. It is felt that given the statistical nature of pore size/spacing in the P/M alloys, regions of material with high porosity likely control the localization and fracture behavior of these alloys. The physical basis of this model (hereafter denoted the SPN analysis) is that there exists across an element of porous material an inclined, planar imperfection of some higher level of

porosity. The element is representative of the bulk material, while the imperfection band is sufficiently thin so as not to contribute to the pre-instability strain of the element. The element of material is subjected to uniform quasi-static deformation and the flow behavior of the imperfection and the surrounding material are computed in accord with the elastoplastic constitutive rate relations for porous materials developed by Gurson (26). Fracture of the material is assumed to be coincident with the development of a localization bifurcation (point at which all continued plastic deformation is constrained to the imperfection) due to accelerated void growth within the imperfection. In order to account for the change in stress state during necking of a tensile specimen, the enhanced stress triaxiality at the center of a neck is incorporated into the analysis via Bridgman's solution (27). The results of this analysis do not take a simple closed form solution, but rather are numerically approximated. The analysis is performed for both uniaxial tension and plane strain tension (for the Ti-6Al-4V) to study the influence of deformation path on instability/fracture. In order to apply the analysis, the imperfection may be assumed to extend across the entire width of the specimen or to extend across a critical length which, upon failure, causes the remaining ligaments to fail. Although the analysis specifically considers the existence of only one imperfection, it must be recognized that a porous engineering material will contain a network of imperfections. Within that network, one surface, or plane, however tortuous its geometry may be, eventually dominates, and causes shear localization, and becomes the fracture path.

Material Preparation

The materials used in this investigation were commercially pure titanium (CP Ti) and Ti-6Al-4V consolidated by P/M techniques. Electrolytically refined titanium sponge (obtained from Dow Howmet Corp.) processed by a

hydride/dehydride method to -80 mesh powder (by Teledyne-Wah Chang Corp.) was used as the base material for both alloys. The Ti-6Al-4V composition was achieved by blending of a 60/40 aluminum-vanadium master alloy powder during processing (by Imperial Clevite Corp.). To obtain the desired range of porosity levels in these two alloys, it was necessary to employ a variety of preparation methods, listed in Table I. The resulting materials contained, on average, 0.1, 0.8 and 3.5% porosity for the Ti-6Al-4V alloy and 0.3, 4.5 and 7.8% porosity for the CP Ti. Full densification of the HIP'ed and swaged material apparently was prevented by the residual chlorine present in the Ti powder (28). After powder fabrication, the porous alloys contained (by weight): $\leq$80ppm Cl, $\leq$150ppm H in the Ti-6Al-4V and $\leq$10ppm H in the CP Ti, .15-.24% O in the Ti-6Al-4V and .13-.15% O in the CP Ti.

Microstructural Characterization

Metallography and fractography were performed on a JEOL JSM 35-C scanning electron microscope. Electron microscopy was used instead of optical microscopy to obtain better resolution of the pore structure on polished surfaces where some pore rounding is unavoidable. The microstructures of the six materials used in this study are shown in Figs. 2 and 3. As can be seen, the porosity is quite rounded. The grain sizes of the Ti-6Al-4V specimens are 94, 89 and 85 μm, respectively, for the 0.1, 0.8 and 3.5% porous materials. For the CP Ti alloys the values are 97, 75 and 69 μm for the 0.3, 4.5 and 7.8% porosity levels. The grain structures of all six materials are equiaxed.

Mechanical Testing

Tensile testing was performed at room temperature at a nominal strain rate of 1.7×10^{-5} sec^{-1}. In order to obtain large strain flow curves for numerical modeling,the Bridgman correction (27) was applied to axisymmetric tests of the 0.1% porous Ti-6Al-4V and the 0.3% porous CP Ti materials via measurements made from sequential photographs of the specimen profile taken

during testing. This approximate analysis was used despite the fact that recent computer simulation studies by Needleman (29), Chen (30) and Norris, Moran, Scudder and Quinones (31) suggest that it somewhat underestimates the magnitude of the stress triaxiality present within the neck of a deforming tensile bar. The resulting data were then least squares fit to two empirical stress-strain equations. The finite element modeling utilized the Swift equation:

$$\bar{\sigma} = K(\bar{\varepsilon}_p + \bar{\varepsilon}_o)^n \quad (1)$$

where K, $\bar{\varepsilon}_o$ and n are constants and $\bar{\sigma}$ and $\bar{\varepsilon}_p$ are the equivalent stress and equivalent plastic strain for an isotropic material(assumed appropriate for our P/M alloys).

The uniaxial stress-strain behavior of the material representative of fully dense alloys with the same microstructures/chemistries as the porous alloys was approximated by the the tensile response of 0.1% porous Ti-6Al-4V and 0.3% porous CP Ti. The appropriate flow curves indicate that the yield strength of the Ti-6Al-4V is more than twice that of the CP Ti (850 vs. 330 MPa) whereas its strain hardening rate, "n" in the Swift equation (eqn. 2), is less than half as large (0.077 vs. 0.188). The plastic flow parameters calculated from these tests and the appropriate elastic constants obtained from the literature (32) are summarized in Table II.

The imperfection analysis of Saje, Pan and Needleman (23) assumes a piecewise power law form for the stress-strain response of the material:

$$\sigma_u = \sigma_y \ (\varepsilon_u/\varepsilon_y) \text{ for } \sigma_u \leq \sigma_y \quad (2)$$

$$\sigma_u = \sigma_y \ (\varepsilon_u/\varepsilon_y)^n \text{ for } \sigma_u > \sigma_y \quad (3)$$

where σ_u and ε_u are the true stress and true strain in uniaxial tension, respectively, σ_y is the yield stress, ε_y is the yield strain ($\varepsilon_y = \sigma_y/E$, where

E is Youngs modulus), and N is a constant. Thus, the experimental stress-strain data were also fit to Eqn's 2 and 3 for purposes of the analysis.

Incremental density measurements were performed on the 4.5% porous CP Ti to determine the void growth rate during tensile straining. Immersion density measurements were performed prior to testing and after each strain increment using the "hydrostatic weighing" method (33). Briefly, this technique determines density by measuring the difference in a specimen's weight in a) air and b) when suspended in a liquid of known temperature and density. The density of the specimen, ρ,is given by

$$\rho = \frac{w_1 \rho_B}{w_1 + w_2 - w_3} \tag{4}$$

where ρ_B is the density of the liquid medium (mono-bromobenzene was used in this study), w_1 is the weight of the specimen in air, w_2 is the weight of the specimen suspension wire dipping into the liquid medium, and w_3 is the weight of the sample and suspension wire immersed in the fluid. The weighings were performed using a Sartorius Selecta single-pan type balance precise to 0.05 mg. The monobromobenzene was contained in a glass vessel immersed in a constant-temperature water bath held at 25 ± 0.1°C. The entire apparatus was located in a temperature and humidity controlled room on an isolation table to minimize fluctuations in the measurements. Testing was stopped prior to maximum load, the gage section removed, and its density measured to provide a basis for scaling earlier measurements (assuming the plastic strain was limited to the gage section).

AN EXPERIMENTAL BASIS FOR AN ANALYSIS

The tensile behavior of materials with pre-existing porosity is characterized by large decreases in both strength and ductility with increasing porosity level (2,3). An example of such behavior is shown in Fig. 4 in which

both the P/M Ti-6Al-4V and CP Ti show a decrease in yield strength (Fig. 4a) as well as tensile ductility (Figs. 4b and 4c) with increasing porosity level. However, the CP Ti with its higher strain hardening capacity proves to be significantly more ductile for a given level of porosity than the low strain-hardening Ti-6Al-4V. All materials tested exhibit a post-maximum load deformation regime followed by an abrupt, catastrophic failure. The data for the 0.1% porous Ti-6Al-4V compares favorably with data for near fully dense Ti-6Al-4V with a different microstructure (34) as well as handbook data for fully dense Ti and Ti-6Al-4V. The similarity of these data to those of the nearly fully dense (0.1% and 0.3% porous) Ti-6Al-4V and CP Ti of this study lends support to the use of these materials to represent the matrix properties of the higher porosity materials. Figure 4 also includes data obtained from plane-strain tensile tests on the Ti-6Al-4V materials. The local fracture strain in plane strain tension is approximately 60% of that in uniaxial tension, independent of the porosity level tested. This compares favorably to previous results for several fully dense materials of similar yield strength levels (35).

In addition to the tensile flow behavior, a critical feature of the fracture of porous materials is the large amount of pre-existing porosity on the fracture surface when compared to bulk porosity levels. Representative fractographs are shown in Figs. 4, 5 and 6 for CP Ti and Ti-6Al-4V axisymmetric tension specimens. The single-phase CP Ti material, with its high strain hardening capacity and good ductility, is characterized by deep dimples and extensive slip markings within pores. In contrast, the low strain hardening two-phase Ti-6Al-4V shows less slip markings and shallow shear dimples. Most important is that in both cases the area fraction of porosity measured from a planar projection of the fracture surface is about eight to ten times the initial porosity level in the bulk; see Table III.

A process which must contribute to the high area fraction of porosity observed on the fracture surface is strain-induced pore growth. Figure 7 shows that for the 4.5% porous Ti, pore growth is nearly linear with strain, consistent with theory (17,25). More significant to the present study is that, given the fracture strains in Fig. 4, the rate of strain-induced pore growth can account for no more than about a 30% increase in pore content at fracture. Even assuming some stress triaxiality due to specimen necking will accelerate pore growth, the high level of porosity (8-10x) on the fracture surface cannot be accounted for by bulk strain-induced pore growth. Thus we conclude that ductile fracture in these porous materials occurs preferentially on planes of high initial pore content.

Finally, it should be noted that, on a microscopic scale, the effect of increasing porosity level is to increase the degree of tortuosity of the fracture path. A qualitative examination of plane strain tension specimens sectioned parallel to their tensile axes shows clearly the increased tortuosity with increasing porosity level as the material attempts to link-up those pores constituting the largest defect in the material.

AN ANALYSIS OF THE DEFORMATION AND FRACTURE BEHAVIOR OF POROUS MATERIALS

A. Yielding and Flow Behavior: Microcell Analysis of Bulk Porosity Effects.

Load-elongation predictions of the finite element microcell model described previously (see Fig. 1) are summarized in Fig. 6, where stress-strain curves for the spherical-cavity microcells at the appropriate densities are compared with experimental curves. For yield stress and small strain calculations, the modeling assumes spherical-cavity microcells. Pore growth measurements (see Fig. 7) indicate reasonable agreement between predictions based on spherical microcells and experimental data at least in the early stages of pore growth. The model clearly underpredicts the observed dependence of strength on porosity,

but properly predicts the observed trends (see Fig. 8). It should also be noted that a simple rule of mixtures which would decrease the yield stress by the volume fraction of porosity would also underestimate the observed decrease in strength with increasing porosity.

Figure 7 summarizes measured and calculated rates of hole growth for 4.5% porous CP Ti in uniaxial tension. The experimentally determined growth rate lies intermediate between the spherical and oblate spheroidal FIPAX microcell predictions, and is about double the rate predicted by the Gurson model (25). The analysis also predicts that the void growth rate is nearly independent of matrix yield stress and work hardening (36), which is in basic agreement with Gurson (25) that void growth is dependent only on the hydrostatic stress component. The FE microcell calculations also predict that the rate of void growth normalized against the initial porosity level is nearly independent of the magnitude of the initial porosity level (26), also consistent with the Gurson model (25).

B. Deformation and Fracture Behavior: An Imperfection Analysis.

The observation that fracture occurs preferentially on "planes" of high pore content clearly suggests that a porous material contains a network of imperfections which eventually trigger a shear instability which dominates flow and causes fracture. As described earlier, the continuum imperfection analysis of Saje, Pan and Needleman [SPN](23) may be used to analyze the fracture behavior of these P/M materials. A difficulty in applying this analysis is in identifying the size of the imperfection present in the material. One possibility is that the pore distribution in our powder consolidated materials can be reasonably inferred from a simple model of the fabrication process.

The scheme used for modeling the pore-induced imperfections is illustrated in Fig. 9. Although the Ti powder used in producing our materials is, in fact, irregular in size and shape, we will approximate it as a close-packed periodic and regular array prior to sintering, shown in Fig. 9b as spheres. Upon sintering, rounded pores are formed at interstitial sites between particles, Fig. 9c. The resulting structure is a periodic array of spherical voids lying along prior particle boundaries. The net effect is that the distribution of porosity formed by P/M consolidation introduces throughout the material an "imperfection network" of material containing much higher than bulk porosity levels.

Depending on the bulk porosity level and the choice of packing polyhedra used to model the powder particles, various levels of porosity can be calculated within the imperfection network. Similar to previous analyses (9,14) the general form of the dependence is:

$$f_p^* = K\, f_p^{2/3} \qquad (5)$$

where f_p^* is the area fraction porosity along prior particle boundaries, f_p is the bulk porosity level and K is a geometric constant dependent on the choice of packing polyhedra with a spherical pore located at each vertex. For cubes, $K \simeq 1.1$ while for tetrakaidecahedra $K \simeq 1.3$. We feel that these models should provide a lower reasonable limit estimate of the surface porosity levels which might be expected to exist in a well-sintered material. In reality, the randomness of porosity in a typical specimen will create planes of high pore content which are quite tortuous as they connect closely spaced pores. As a consequence, the level of porosity predicted by Eq. 5 is a lower level estimate; experimentally observed values should be higher. This is confirmed by the comparison between observed levels of porosity and those predicted from Eq. 5 as shown in Table III. The pore contents predicted from Eq. 2 are at least a factor of two lower than those observed.

As has already been pointed out, the void growth rates predicted by the Gurson constitutive model are lower than those measured; see Fig. 7. To correct for this, the finite-element predicted growth rates from the microcell analysis (Fig. 5, also ref. 37) were used to modify the Gurson model (26) using techniques described elsewhere (21,38). This procedure matches the initial growth rates of the SPN analysis (23) and the finite element predictions. However, the growth rates accelerate more rapidly in the bifurcation analysis than in the finite element results. The result is that the predicted localization (and fracture) strains are less than those predicted from the imperfection analysis based on the original Gurson model (Fig. 10). When compared to Fig. 10, the resulting agreement between the modified theory and experimental observations is improved somewhat for the Ti-6Al-4V but is worse for the CP Ti.

That the imperfection network described above is the defect responsible for flow localization/fracture in P/M consolidated materials is also supported by the results of the SPN analysis (23), shown in Fig. 10. The solid lines in Fig. 10 represent the mean predicted instability strains for the bounding values indicated by triangle and square symbols. The agreement is found to be quite good for the CP Ti materials over the full range of porosity levels examined. The model also successfully predicts the ductility of the 3.5% porous Ti-6Al-4V material. Only at small (<1%) porosity levels in the Ti-6Al-4V is there poor agreement between theory and experimental data.

The imperfection analysis also clearly predicts the stabilizing influence of increasing work hardening in resisting flow localization and failure in porous materials. This can be seen by comparing the theoretical values of $\bar{\varepsilon}_f$ for Ti-6Al-4V vs. CP Ti in Fig. 10. For example, Fig. 10 shows that, at 5% porosity, an imperfection ratio of 3 (f_p^*/f_p) would result in an instability strain of 0.08 in Ti-6Al-4V but 0.20 in the CP Ti. This difference is due to

the high work hardening exponent of CP Ti ("n" in the Swift equation is .188 vs. 077 for Ti-6Al-4V).

DISCUSSION

The experimental behavior and the analyses presented indicate that the deformation and fracture behavior of porous metals may be understood on two levels: bulk porosity and local porosity effects. In particular, fracture, and possibly flow behavior as well, appear to be dominated by effects caused by the distribution of porosity on a local scale.

The principal observation with respect to the flow stress behavior in the P/M consolidated materials studied is that, in general, the flow stress decreases with porosity at a rate which is much more rapid than is predicted by either the FE microcell analysis (see Fig. 1) or a rule of mixtures calculation. This effect is typical of sintered, porous metals (2,3), and several analyses have been suggested, most of these being based on elastic stress concentrations and on the level of porosity on planes of high pore content assuming a periodic array of pores (2,3). This seems overly simplistic but neither the microcell nor the imperfection analysis is able to predict this effect in their present form.

While the microcell analysis is quite adequate for predicting mean void growth rates in which the behavior of large numbers of pores are averaged, it cannot account for behavior controlled by local porosity. This occurs as a consequence of the assumed idealized pore distribution consisting of a periodic, regular array of equal sized voids with an AAA... stacking sequence. Such a distribution maximizes near-neighbor distances and thus minimizes local pore interactions. By way of contrast, the pore structures in the actual P/M alloys allow a given pore to interact with much nearer neighbors. Interaction will thus proceed primarily between those pores with the most favorable

relative positions and shapes, particularly in clusters, to allow deformation of the joining ligament. It seems likely that such ligaments would be preferential sites of straining throughout the deformation history of the sample and that they would ultimately constitute the fracture surface.

The fact that the area fraction of pores in the plane along which fracture occurs is eight to ten times that in the bulk material clearly indicates that the fracture process is controlled by the non-uniformity of pore distribution, specifically by bands of locally high porosity which act as imperfections. Comparison of the calculated and observed results in Fig. 10 show that the SPN analysis (23), which is based on a pre-existing imperfection, is in good agreement with nearly all of the observed results. Poor agreement at small porosity levels is to be expected since the SPN analysis requires an imperfection for failure; thus for fully dense material with no pores (and no imperfection in our case) the analysis will tend to overpredict the ductility.

In addition to the above major factor, there are also several other factors which will limit the accuracy of the SPN calculations in predicting the ductility of P/M alloys. Choice of imperfection size has already been mentioned and is clearly a difficulty, although the upper and lower limit methods used for Fig. 10 seem to be reasonable estimates. More subtle are the effects of pore distribution in diffusing slip and in accelerated void growth and stress/strain localization between voids. In the SPN analysis, the planar imperfections, which have a well-defined interface with the matrix, yield before the adjacent bulk material and continue to maintain higher strain levels until instability occurs. In a porous material, as straining proceeds there will be a constant competition for deformation to occur, from large pores or groups of pores (or other "imperfections") which, while they possess the necessary characteristics for easy deformation, do not lie on a surface sufficiently defective so as to comprise the final fracture surface.

Given the "single void" model of Gurson used in the imperfection analysis, an additional limit is the presence of accelerated pore/void growth and stress/strain localization within clusters of voids contained within the imperfection. As has been shown by the comparison between the FE microcell model and the Gurson model predictions, Fig. 7, void growth appears to be enhanced by the presence of neighboring voids. This effect was examined in the SPN analysis based on the modified Gurson model discussed previously. The result was a significant decrease in localization strain at a given pore content. In addition strain localization within clusters of pores definitely promote strain gradients within the imperfection, and these gradients will be responsible for failure occurring at a lower average matrix strain than would be predicted on the basis of the Gurson analysis, where such strain gradients are neglected.

The effect of strain rate sensitivity on instability is the final factor which limits the SPN analysis. A recent analysis due to Pan, Saje and Needleman (39) indicates that the incorporation of positive rate sensitivity in the imperfection analysis can delay the onset of instability in porous materials. The actual effect of rate sensitivity could be even larger than predicted by the imperfection analysis, given the strain gradients present within intervoid ligaments. As these regions deform faster than assumed in the Gurson model, they will experience a larger stabilizing influence due to positive strain rate hardening.

Conclusions

This study has examined the microstructural and mechanical parameters which control the deformation and fracture behavior of porous high strength engineering alloys. The experimental behavior of two P/M Ti alloys possessing different strain hardening characteristics and containing various levels of porosity has been modeled on a bulk porosity basis using a large strain FE

analysis and on a local porosity scale utilizing a continuum imperfection analysis. The FE model is in reasonable agreement with the measured values of void growth but underestimates the observed degradation of strength with increasing porosity level. In large part, this appears to be due to the excessive stiffness of the "microcell" model used and the presence of a network of imperfections within the material due to random nature of the pore distribution.

In a novel approach to examining the influence of porosity on the ductility of P/M alloys, a continuum imperfection model has been used to analyze measured values of tensile ductility. The imperfections take into account variations in local pore content and consist of planes of weakness containing a higher-than-bulk density of pores. Direct evidence for the presence of such planes is the observation that the observed porosity on the fracture surface is much greater than that in the bulk even taking into account strain-induced pore growth. A minimum size of the imperfection is estimated by considering a periodic array of powder particles which, upon sintering, form an imperfection network with an area fraction f_p^* of porosity along the prior particle boundaries related to the bulk porosity level f_p by $f_p^* \alpha f_p^{2/3}$. Although the imperfection theory used is limited by simplifying assumptions, it is in reasonable agreement with experimental observations. Finally it should be noted that the analysis also predicts the stabilizing influence of strain hardening on flow localization and failure in porous materials.

ACKNOWLEDGEMENTS

The authors wish to thank Prof. A. Needleman for providing the imperfection analysis computer program used in this study, Dr's. W. A. Spitzig and M. E. Devenpeck for stimulating discussions, and Dr. E. N. Aqua, Mr. V. Moxson, and Imperial Clevite Co. for assistance in materials preparation. This research was supported by the Office of Naval Research through Contract No. N00014-76-C-0037, NR 031-76.

TABLE I

Processing schedules used to prepare Ti-6Al-4V and CP Ti test materials.

Alloy	%porosity	compaction method/pressure(MPa)		sinter*** temp(°C)/time(hr)		additional
Ti-6Al-4V	0.13	Die	620	1325	4	HIP* 925°C/ 103 MPa/ 2 hr.
Ti-6Al-4V	0.85	Die	620	1325	4	------
Ti-6Al-4V	3.5	Die	620	1325	4	------
CP Ti	0.3	CIP**	276	1400	4	Swage 50%RA H.T.1400°C/ 4 hr.
CP Ti	4.5	Die	690	1400	4	------
CP Ti	7.8	CIP**	276	1400	4	------

*HIP denotes hot isostatic pressing

**CIP denotes cold isostatic pressing

***sintering performed under a dynamic vacuum of 10^{-5} mm Hg

TABLE II

Mechanical parameters used in the finite element modeling and continuum imperfection analyses.

	Ti-6Al-4V	CP Ti
E (Youngs Modulus) MPa	110×10^3	110×10^3
ν (Poissons ratio)	0.33	0.33
K, MPa	1277.10	688.07
ε_o	0.0056	0.0190
n	0.0773	0.1885
σ_y MPa	858.43	211.68
ε_y	0.0078	0.0019
N	0.0843	0.1882

TABLE III. Initial bulk porosity contents (a) as compared to the porosity levels determined (b) on the fracture surface (as measured by a planar projected), and (c) along a plane of high pore content as predicted by Eq. (5).

Volume or Area Fraction Porosity	Ti-6Al-4V		CP Ti	
(a) Initial bulk measurement	0.0085	0.035	.045	.078
(b) On fracture surface	.09	.30	.42	.56
(c) Along imperfection as predicted from $f_p^* = kf_p^{2/3}$ (Eq. 5)	.05	.12-.14	.14-.16	.20-.24

REFERENCES

1. S. H. Goods and L. M. Brown, Acta Metall. 27, 1 (1979).

2. R. Haynes, The Mechanical Behavior of Sintered Alloys, Freund Publishing House, London, 1981.

3. B. Karlsson and I. Bertilsson, Scand. J. of Met. 11, 267 (1982).

4. B. I. Edelson, Trans. ASM 56, 82 (1963).

5. B. I. Edelson, Trans. ASM, 56, (1963) 82-89.

6. M. Perra and I. Finnie, in Fracture 1977, Vol. 2, p. 415, Univ. of Waterloo Press, Waterloo, 1977.

7. R. J. Bourcier and D. A. Koss, in Advances in Fracture Research, Vol. 1, p. 187, Pergamon Press, London, 1982.

8. R. J. Bourcier, R. E. Smelser, O. Richmond and D. A. Koss, Intern. J. of Fracture 24, 289 (1984).

9. M. Eudier, Powder Metall. 6, 278 (1962).

10. B. I. Edelson and W. M. Baldwin, Trans. ASM 55, 230 (1962).

11. A. Salak, V. Miskovič, E. Dubrová, E. Rudnayoua, Powder Metall. Intern. 6, 128 (1974).

12. R. Haynes, Powder Metall. 20, 17 (1977).

13. H. E. Exner and D. Pohl, Powder Metall. Intern. 10, 193 (1978).

14. T. J. Griffiths, R. Davies, and M. B. Bassett, Powder Metall. 22, 119 (1979).

15. N. A. Fleck and R. A. Smith, Powder Metall. 24, 126 (1981).

16. F. A. McClintock, J. Appl. Mech. 35, 363 (1968).

17. J. R. Rice and D. M. Tracey, J. Mech. Phys. Solids 17, 201 (1969).

18. A. Needleman, J. Appl. Mech. 35, 964 (1972).

19. A. Melander, Acta Met. 28, 1799 (1980).

20. P. F. Thomason, Acta Metall. 29, 763 (1981).

21. V. Tvergaard, Intern. J. Frac. 17, 389 (1981) and 18, 237 (1982).

22. E. J. Appleby, R. E. Smelser, and O. Richmond, unpublished research; see Final Report, U.S. Army Research Office, Contract DAAG 29-78-C-0008.

23. M. Saje, J. Pan, and A. Needleman, Intern. J. of Fracture 19, 163 (1982).

24. J. R. Osias, unpublished research.

25. H. Yamamoto, Intern. J. Frac. 14, 347 (1978).

26. A. L. Gurson, J. Engr. Matl's. and Tech. 99, 2 (1977).

27. P. W. Bridgeman, Studies in Large Plastic Flow and Fracture, p. 9, McGraw-Hill, New York, 1952.

28. A. G. Jackson, J. Moteff, and F. H. Froes in Powder Metallurgy of Titanium Alloys, p. 229, The Met. Soc. of AIME, Warrendale, PA, 1980.

29. A. Needleman, J. Mech. Phys. Solids 20, 111 (1972).

30. W. H. Chen, Intern. J. Solids and Structures 7, 685 (1971).

31. D. M. Norris, B. Moran, J. K. Scudder, and D. F. Quinones, J. Mech. Phys. Solids 26, 1 (1978).

32. Metals Handbook, Ninth Edition, ASM, Metals Park, OH, 1979.

33. F. Garafalo and H. A. Wriedt, Acta Metall. 10, 1007 (1962).

34. P. J. Anderson, V. M. Svoyatytsky, F. H. Froes, Y. Mahajan, and D. Eylon, in Modern Developments in Powder Metallurgy, p. 537, Met. Powder Ind. Fed., Princeton, NJ, 1982.

35. D. P. Clausing, Intern. J. Frac. Mech. 6, 71 (1970).

36. R. E. Smelser and O. Richmond, unpublished research.

37. R. J. Bourcier, Ph.D. Thesis, Michigan Technological University, Houghton, MI, 1983.

38. R. Becke, R. E. Smelser, and O. Richmond, unpublished research.

39. J. Pan, M. Saje, and A. Needleman, Intern. J. of Fracture 21, 261 (1983).

List of Figures

Figure 1. A schematic illustration of the formulation scheme for the finite element microcell model.

Figure 2. Scanning electron micrographs of CP Ti containing (a) 0.3, (b) 4.5 and (c) 7.8% porosity.

Figure 3. Scanning electron micrographs of Ti-6Al-4V containing (a) 0.1, (b) 0.8, and (c) 3.5% porosity.

Figure 4. The influence of porosity on (a) the yield stress σ_y, (b) the elongation to failure e_f, and (c) the percent reduction in area %R.A. for CP Ti. All data is from tests in uniaxial tension except for the plane strain P.E. tests of Ti-6Al-4V in (c).

Figure 5. Scanning electron fractographs of (a) 0.3, (b) 4.5, and (c) 7.8% porous CP Ti.

Figure 6. Scanning electron fractographs of (a) 0.1, (b) 0.8, and (c) 3.5% porous Ti-6Al-4V tested in uniaxial tension.

Figure 7. Measured and predicted normalized rates of void growth for a CP Ti tensile specimen containing 4.5% porosity. The predictions are based on either the Gurson model (26) or the finite element microcell model.

Figure 8. Engineering stress-strain curves for (a) CP Ti and (B) Ti-6Al-4V as measured experimentally (Exp) and as predicted from the finite element microcell model (FE).

Figure 9. A schematic illustration of an idealized pore distribution based on (a) packing of hydride/dehydride powder used in this study as simulated by (b) an idealized packing of spherical powder particles and (c) a rounded pore structure obtained after sintering.

Figure 10 The influence of porosity on the strain to fracture of Ti-6Al-4V and CP Ti as determined experimentally and as predicted from the SPN analysis (23) assuming the area fraction of porosity within the imperfection f_p^* is related to that in the bulk f_p by either $f_p^* = (1.1 \text{ or } 1.3) f_p^{2/3}$.

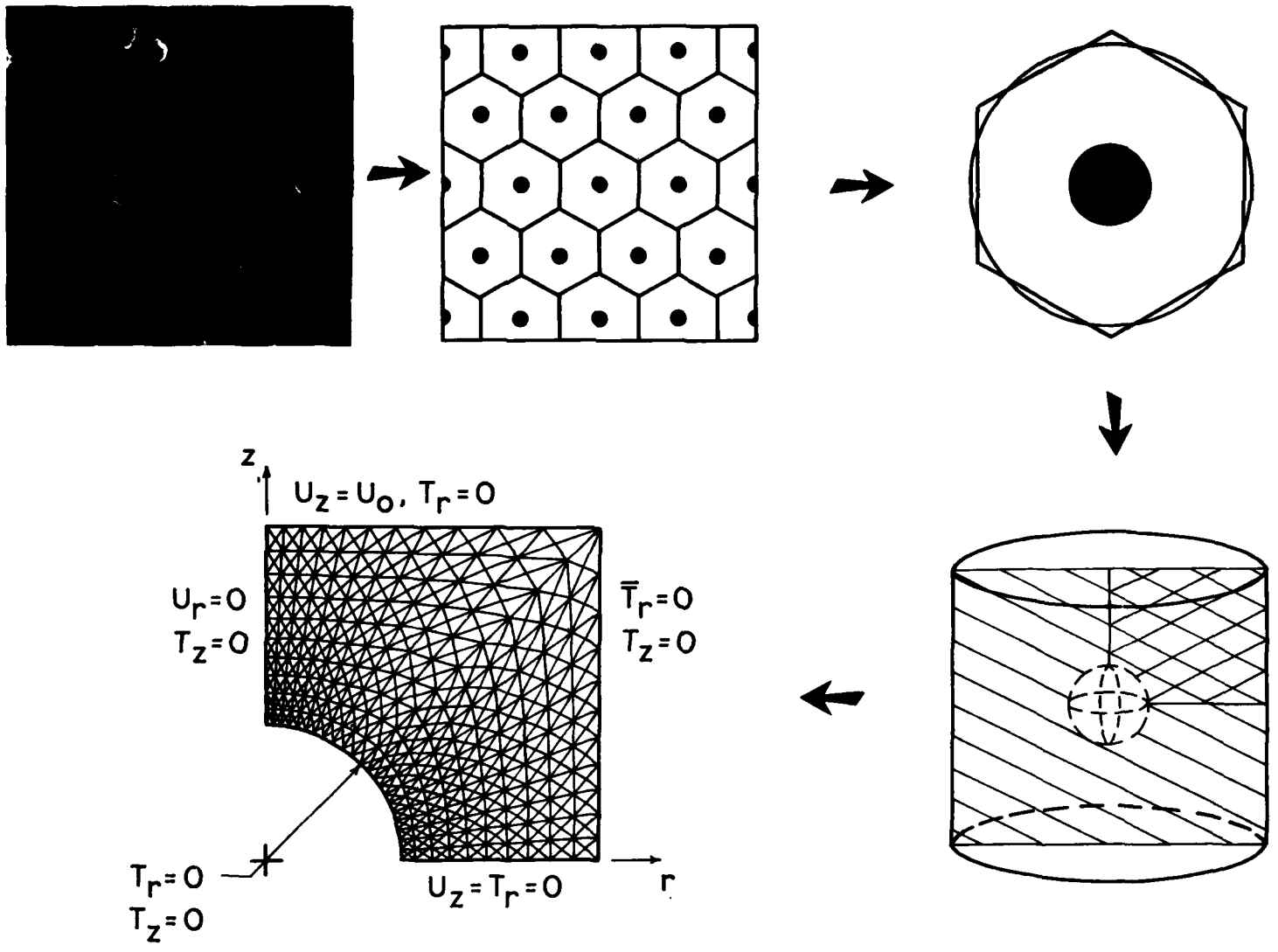

Figure 1. A schematic illustration of the formulation scheme for the finite element microcell model.

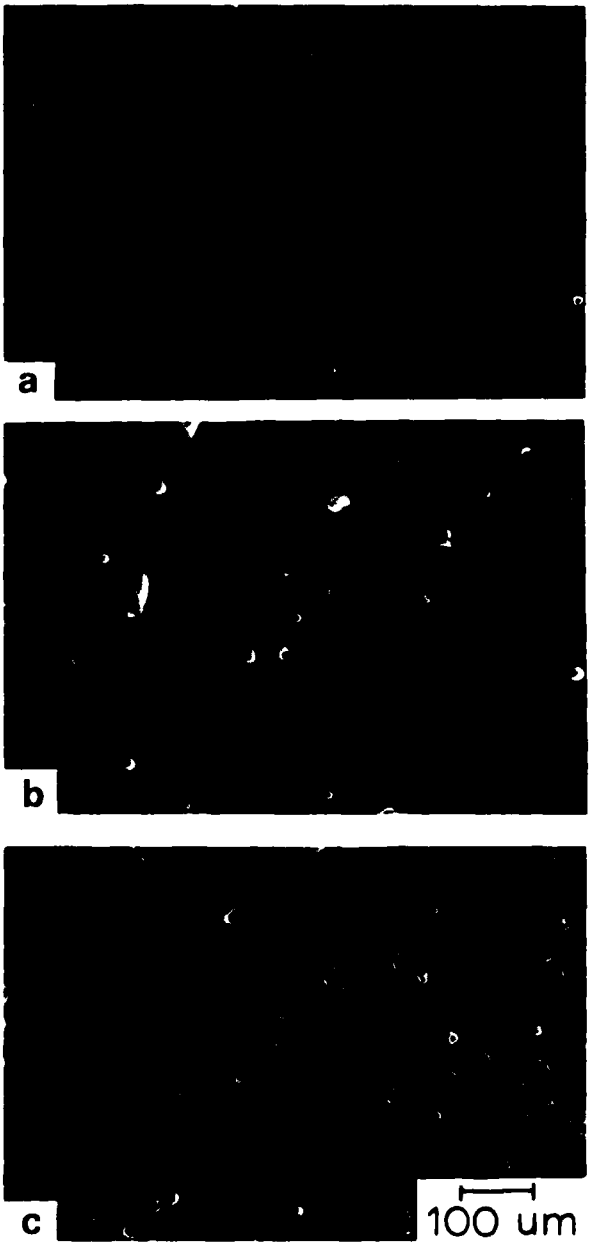

Figure 2. Scanning electron micrographs of CP Ti containing (a) 0.3, (b) 4.5 and (c) 7.8% porosity.

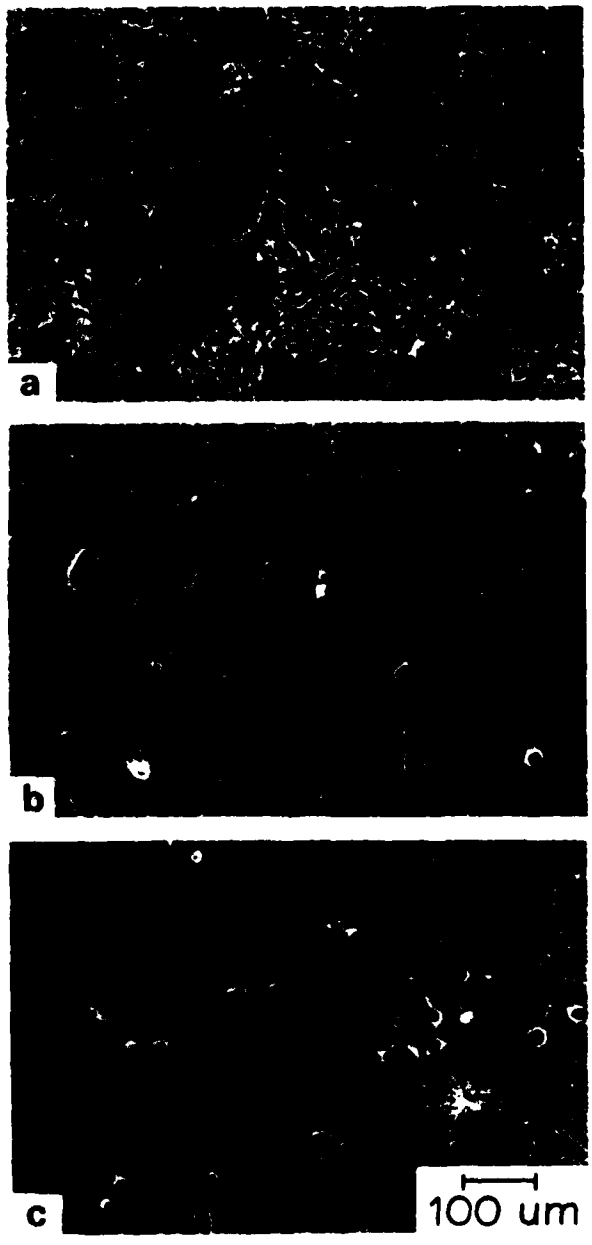

Figure 3. Scanning electron micrographs of Ti-6Al-4V containing (a) 0.1, (b) 0.8, and (c) 3.5% porosity.

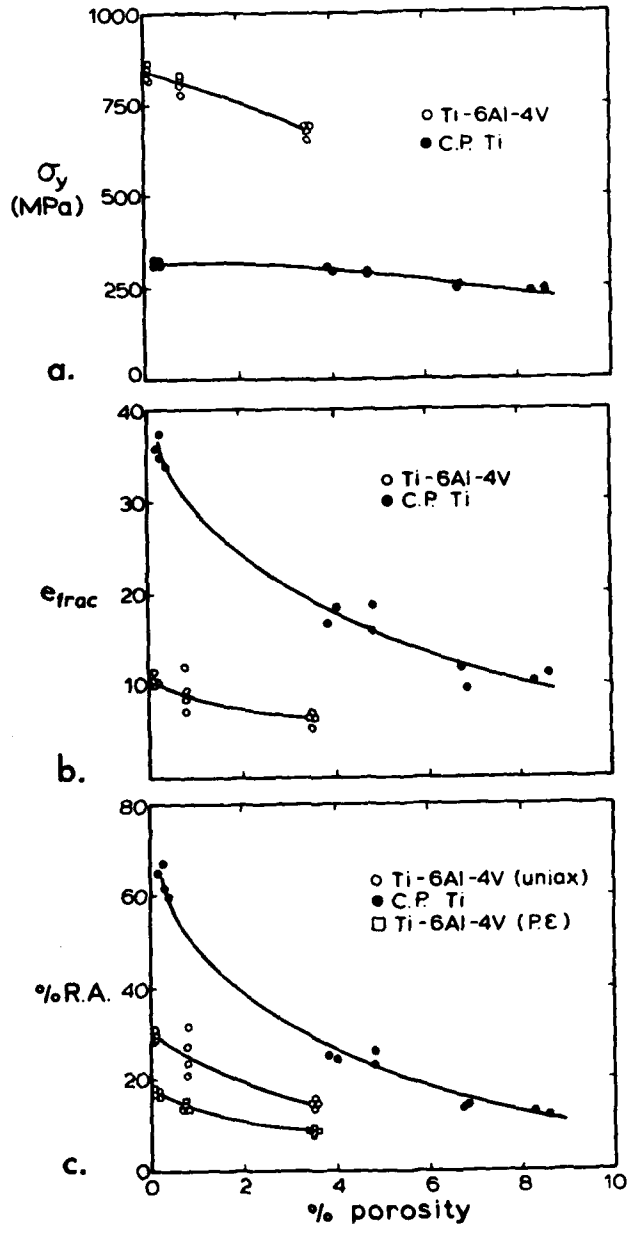

Figure 4. The influence of porosity on (a) the yield stress σ_y, (b) the elongation to failure e_f, and (c) the percent reduction in area %R.A. for CP Ti. All data is from tests in uniaxial tension except for the plane strain P.E. tests of Ti-6Al-4V in (c).

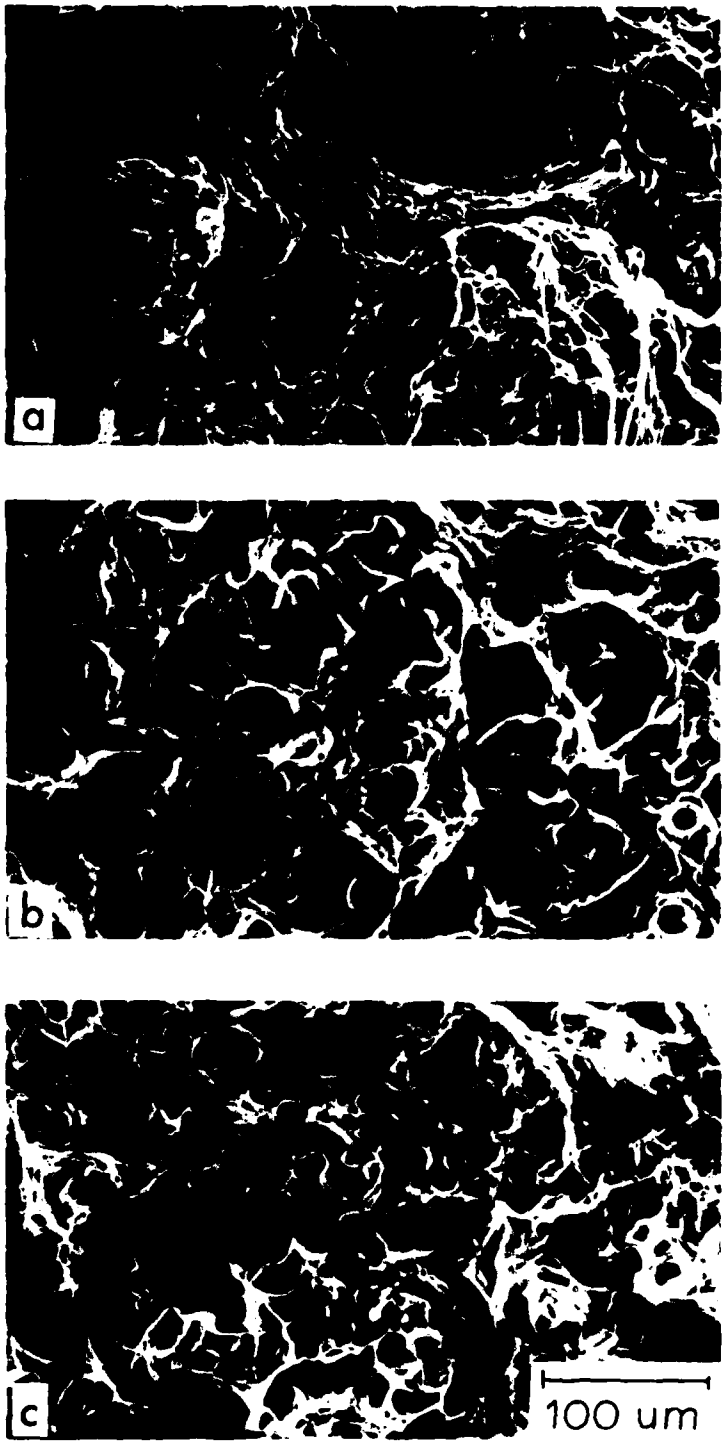

Figure 5. Scanning electron fractographs of (a) 0.3, (b) 4.5, and (c) 7.8% porous CP Ti.

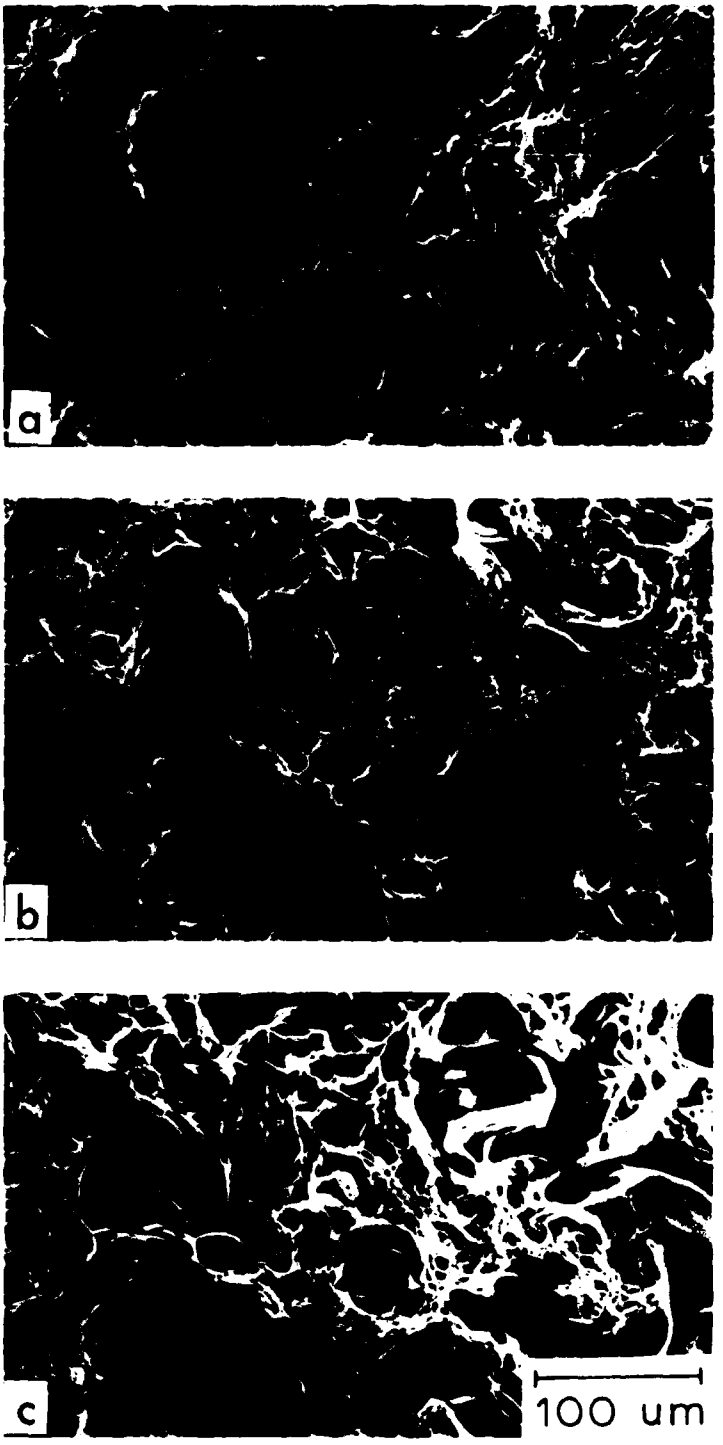

Figure 6. Scanning electron fractographs of (a) 0.1, (b) 0.8, and (c) 3.5% porous Ti-6Al-4V tested in uniaxial tension.

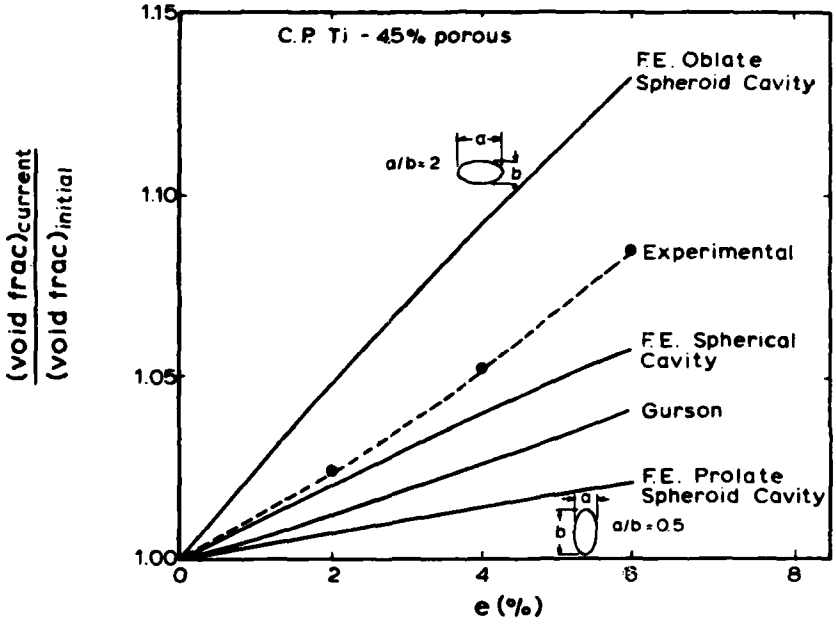

Figure 7. Measured and predicted normalized rates of void growth for a CP Ti tensile specimen containing 4.5% porosity. The predictions are based on either the Gurson model (26) or the finite element microcell model.

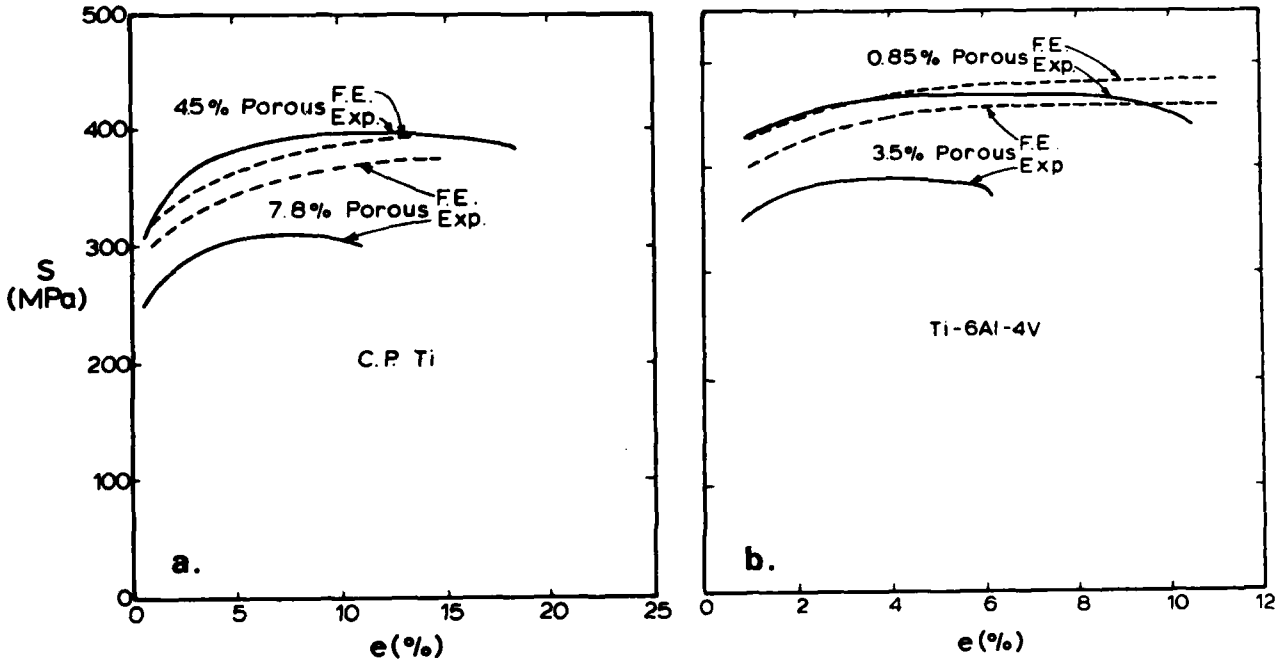

Figure 8. Engineering stress-strain curves for (a) CP Ti and (B) Ti-6Al-4V as measured experimentally (Exp) and as predicted from the finite element microcell model (FE).

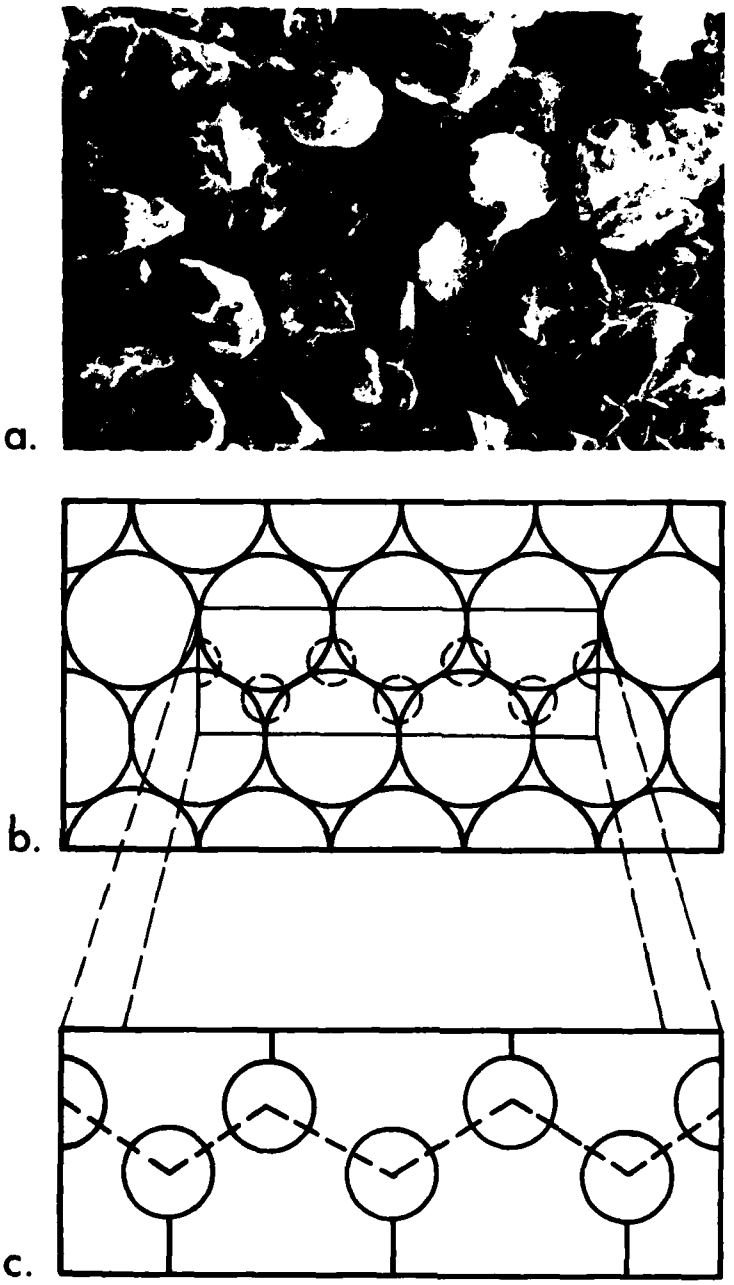

Figure 9. A schematic illustration of an idealized pore distribution based on (a) packing of hydride/dehydride powder used in this study as simulated by (b) an idealized packing of spherical powder particles and (c) a rounded pore structure obtained after sintering.

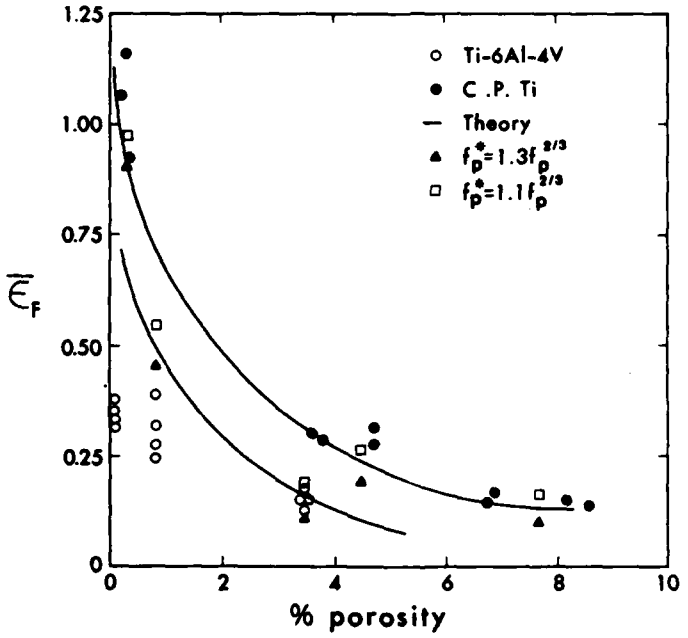

Figure 10 The influence of porosity on the strain to fracture of Ti-6Al-4V and CP Ti as determined experimentally and as predicted from the SPN analysis (23) assuming the area fraction of porosity within the imperfection f_p^* is related to that in the bulk f_p by either $f_p^* = (1.1 \text{ or } 1.3) f_p^{2/3}$.

END

FILMED

1-85

DTIC